Soft Embossing of Nanoscale Optical and Plasmonic Structures in Glass

Jimin Yao,[†] An-Phong Le,[†] Matthew V. Schulmerich,[‡] Joana Maria,[§] Tae-Woo Lee,[⊥] Stephen K. Gray,[¶] Rohit Bhargava,[‡] John A. Rogers,[†,§] and Ralph G. Nuzzo[†,§,*]

[†]Department of Chemistry, [‡]Department of Bioengineering, Beckman Institute, [§]Department of Materials Science and Engineering, Frederick Seitz Materials Research Laboratory, University of Illinois at Urbana—Champaign, Urbana, Illinois 61801, United States, [⊥]Center for Computation & Technology, Louisiana State University, Baton Rouge, Louisiana 70803, United States, and [¶]Center for Nanoscale Materials, Argonne National Laboratory, Argonne, Illinois 60439, United States

ABSTRACT We describe here soft nanofabrication methods using spin-on glass (SOG) materials for the fabrication of both bulk materials and replica masters. The precision of soft nanofabrication using SOG is tested using features on size scales ranging from 0.6 nm to 1.0 μm. The performance of the embossed optics is tested quantitatively *via* replica patterning of new classes of plasmonic crystals formed by soft nanoimprinting of SOG. These crystals are found to offer significant improvements over previously reported plasmonic crystals fabricated using embossed polymeric substrate materials in several ways. The SOG structures are shown to be particularly robust, being stable in organic solvent environments and at high temperatures (~450 °C), thus extending the capacities and scope of plasmonic crystal applications to sensing in these environments. They also provide a stable, and particularly high-performance, platform for surface-enhanced Raman scattering. We further illustrate that SOG embossed nanostructures can serve as regenerable masters for the fabrication of plasmonic crystals. Perhaps most significantly, we show how the design rules of plasmonic crystals replicated from a single master can be tuned during the embossing steps of the fabrication process to provide useful modifications of their optical responses. We illustrate how the strongest feature in the transmission spectrum of a plasmonic crystal formed using a single SOG master can be shifted precisely in a SOG replica between 700 and 900 nm for an exemplary design of a full 3D plasmonic crystal by careful manipulation of the process parameters used to fabricate the optical device.

KEYWORDS: surface plasmon resonance · surface-enhanced Raman scattering · soft lithography · organic sensing · nanostructure · finite-difference time-domain · plasmonic crystal

The fabrication of ordered nanostructures is an important capability required to sustain progress in many areas of modern science and technology. It is critical for technologies exploiting the optical, photonic, and electronic properties of materials. As a result, numerous patterning methods have been actively investigated to overcome the limitations associated with conventional photolithographic technologies typically used to construct such structures.[1−19] Soft lithography, encompassing many flexible methods, has become one of the most robust and versatile nonphotolithographic routes to nanofabrication.[20] Soft lithographies are physical means of patterning that use a patterning tool—such as a stamp, mold, or mask made of a flexible elastomer that ensures both conformal contact between surfaces of the patterning tool and the substrates of interest as well as easy release of the substrate without destruction of the structures formed—to effect a desired form of pattern transfer. By applying different methods of soft lithography, nanostructures with challenging feature sizes, even those reaching molecular level dimensions, have been transferred successfully to a variety of materials.[21−25] In the present work, we explore the use of a specific form of soft lithography, soft embossing, as a means for fabricating with high precision challenging nanostructures in hard materials, and we provide specific demonstrations of means for fabricating useful plasmonic optics with enhanced responsiveness at visible wavelengths.

Surface plasmon resonance (SPR) sensors based on nanostructured metal films and plasmonic crystals, the testbed for this work, has attracted significant attention recently thanks to their high sensitivity in local refractive index sensing and the possibility of their integration into low-cost, portable, imaging-based devices.[1,26−29] Such sensors provide a high-performance platform for label-free forms of analytical detection and field-enhanced applications including surface-enhanced Raman scattering (SERS)[30−34] and surface-enhanced fluorescence.[35−38] Nanostructured SPR devices have more recently found roles in renewable energy where they can be used to enhance light trapping in photovoltaic devices.[39−42] The practical fabrication of nanostructured plasmonic sensors with reproducible performance requires techniques that can be used to generate ordered nanostructures over large substrate areas with high fidelity and control at low cost. The design rules for these optical systems are

* Address correspondence to r-nuzzo@illinois.edu.

Received for review April 20, 2011 and accepted June 16, 2011.

Published online June 28, 2011
10.1021/nn201464t

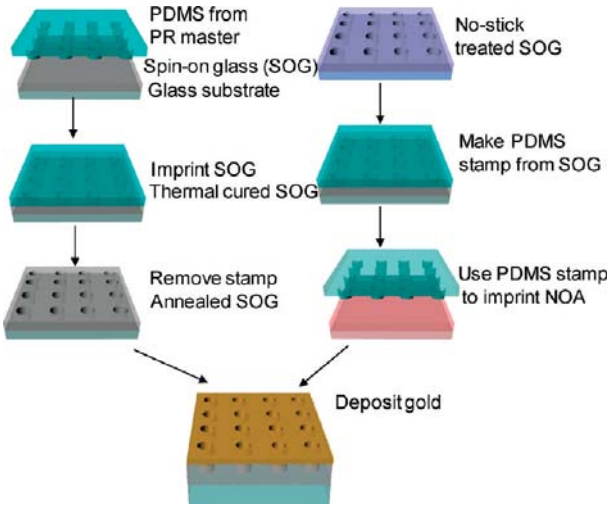

Figure 1. Schematic illustration of the fabrication of SOG-based plasmonic crystals (left) and the NOA-based plasmonic crystals using a SOG-embossed nanostructure as the master (right).

quite demanding and challenging to realize in practice. Most current fabrication methods are commonly based on conventional photolithography technologies,[43−48] and other complementary methods such as nanosphere lithography,[11,12] soft interference lithography,[13,14,49−51] and soft nanoimprint lithography.[21,22]

We have developed classes of plasmonic crystal systems based on periodic arrays of cylindrical nanoholes embossed in polymer films using soft nanoimprint lithography.[27−29,52,53] These nanostructured plasmonic crystals provide high sensitivity in both quantitative multispectral sensing modes and SPR imaging at near-infrared and visible wavelengths.[1,27,29] The sensitivity enhancement seen at visible wavelengths with specific plasmonic crystal design rules is subject to useful forms of tuning *via* modifications made to the distribution and thickness of metal films deposited on the embossed plasmonic crystal substrate, all while keeping the underlying design attributes of the substrate nanostructures constant.[29]

The polymer based plasmonic crystals we previously developed are exceptionally high performance sensing devices[27,29,30,52−54] but are restricted in important ways by their limited stability in many organic solvents or at temperatures higher than the glass transition temperature of the polymers themselves, imposing limits on the scope of any potential sensing applications. Additionally, the polymer and photoresist based systems we have previously used in the fabrication of the plasmonic crystals have a limited refractive index range (n = 1.56 − 1.60).[27,29,30] Just as changes in the refractive index of the local environment generate changes in the optical properties of the plasmonic sensor, it should be expected that the refractive index of the embossing medium also exerts similar control over the optical properties and the plasmonic modes supported by the sensor.

We also have found that the elastomer stamps used in soft nanoimprinting degrade over time due to the absorption of nonpolar monomers within the elastomer, leading to a gradual drift in feature sizes upon reuse and a lifetime for replication limited to ∼10 generations. This places a large demand on the original lithographic masters which themselves, for the feature sizes associated with optics useful for imaging based sensing at visible wavelengths, cannot be reused more than *ca.* 5−6 times without significant degradation. This is a considerable disadvantage because the fabrication of the original lithographic masters with their precise nanometer feature sizes requires advanced photolithography techniques. For these reasons, there exists an important need to develop more robust materials that provide comparable facilities for high resolution, low defect patterning by soft embossing. This paper describes a comprehensive study made to this end.

We introduce here the application of inorganic spin-on glass (SOG) materials for use as a high resolution thermoset embossing medium, a materials choice that greatly enhances both the durability and stability of embossed nanoscale structures while simultaneously facilitating their ease of manufacture. Experimental findings obtained using these new plasmonic sensors reveal that the inorganic material is stable even when exposed to organic solvents and high temperatures. We also demonstrate that embossed SOG materials can serve as durable and regenerable masters for the fabrication of new plasmonic nanostructures, reducing the demand for expensive photolithographic masters and potentially decreasing the cost of plasmonic crystal fabrication. We further demonstrate that these inorganic molded plasmonic nanostructures provide significant improvements over plasmonic crystals fabricated using embossed organic polymers for SERS measurements.[30,55−60] In this paper, the replication

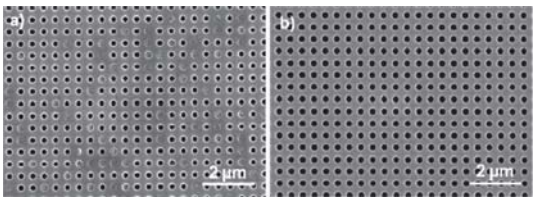

Figure 2. Top view scanning electron microscopy (SEM) images of the plasmonic crystal nanostructure with periodicity of ~580 nm and hole diameter of ~300 nm embossed in (a) NOA film and (b) SOG film.

precision of SOG materials is examined from the micrometer to the near-molecular level. The usage of SOG materials improves the fabrication process of plasmonic crystals and provides a low-cost, simple route to optimize the device form factors with the assistance of finite-difference time-domain (FDTD) calculations.

RESULTS AND DISCUSSION

Nanofabrication Using SOG as a Molding Material. The left side of Figure 1 schematically illustrates the procedures for fabricating plasmonic crystals from SOG masters. A h-PDMS/s-PDMS composite stamp with surface relief structure replicated from a photolithographic master was used to emboss the SOG sol. The stamp is driven into the soft sol by gravity under a modest load to achieve conformal contact, soft baked at 110 °C for 3 min, and then carefully removed. The embossed SOG was then fully cured by a series of higher temperature bakes. A SOG plasmonic crystal can be generated by depositing a 5 nm SnO_2 adhesion layer followed by a 35 nm Au film on top of the embossed nanostructures *via* sequential sputter depositions carried out in 5 mTorr argon environments.

Substituting a high optical quality spin-on-glass resin for the photocurable polymer improves the replication quality of the fabrication protocol. The subsequent separation of the PDMS stamp from the SOG sol is surprisingly easy, sufficiently so as to enable the fabrication of small features with high precision and quality. For example, the smallest nanohole arrays with hole diameters of 240 nm in our design rule are difficult to replicate using polymeric photocurable materials (Figure 2a), but these small features are easily replicated in SOG (Figure 2b).

The materials chemistry of SOG itself is the most challenging aspect of using it as an embossing material and care must be taken to avoid chemical degradation which leads to the formation of gross structural defects. Specifically, the SOG precursor materials are sensitive to moisture and subject to as yet poorly predictable forms of degradation that destroy their capacity to effect precise replication with nanometer design tolerance. We noticed in our experiments, for example, that nanoparticles with sizes around 50 nm frequently appeared on the surface of the embossed SOG nanostructure, decreasing the quality of the plasmonic nanostructure replication (Supporting Information, Figure SI 1a,c). Filtering the SOG sol using 0.22 and 0.02 μm syringe filters before spin-casting removes these nanoparticles very effectively and produces embossed SOG nanostructures with smooth surfaces (Supporting Information, Figure SI 1b,d). It is clear that there are no particles on the surface of filtered SOG films while numerous particles occupy the surface of the unfiltered SOG films. The particle-free regions of the surface coming from unfiltered SOG are as smooth as those of the filtered SOG film, suggesting the nanoparticles are formed and suspended *via* adventitious hydrolysis.

SOG embossed nanostructures can serve as durable masters for the replication of plasmonic crystals following the procedure depicted on the right side of Figure 1. Generally, a monolayer of a fluorinated silane release agent is formed on the embossed SOG surface to promote the separation between the SOG and the cast PDMS. After forming this self-assembled monolayer, a composite h-PDMS/s-PDMS stamp is cast and cured to replicate the SOG embossed structure. The resultant PDMS stamp can be used to emboss photocurable materials to generate plasmonic nanostructures. For example, photocurable NOA was molded using a PDMS stamp with a relief structure replicated from a SOG master. The data in Figure 3 show that these replicated stamps maintain fidelity with the original lithographic master, yielding large area NOA supported nanohole arrays with high replication precision.

Fabrication and Spectral Tuning of Plasmonic Crystals Molded in SOG. The SOG master can also provide an easy way to tune the design rule of the plasmonic crystals (Supporting Information, Figure SI 2). Shrinkage of SOG upon curing during the SOG embossing process results in nanohole arrays embossed on the SOG surface with enlarged nanohole diameters and reduced relief depths compared to the original photolithographic master. We found somewhat surprisingly that the relief depth can be tuned by controlling the solvent evaporation conditions during the embossing of the SOG sol. For example, the embossed SOG nanostructure will have a shallower relief depth when the solvent is evaporated from the spin-coated SOG sol before embossing compared with that of the embossed SOG nanostructure imprinted by PDMS immediately after the SOG sol is cast on the glass slide.

As an illustration of this latter design-centric capability, we first fabricated an NOA-based 3D plasmonic crystal[29] with strong transmission mode optical features located at ~700 nm using a SOG master with a relief depth of ~200 nm. The topography of this plasmonic crystal design was measured using atomic force microscopy (AFM), and an inverted 3D representation of the surface confirming the ~200 nm relief depth is presented in Figure 3a. Normal-incidence transmission spectra for this NOA-based plasmonic crystal nanostructure obtained both experimentally

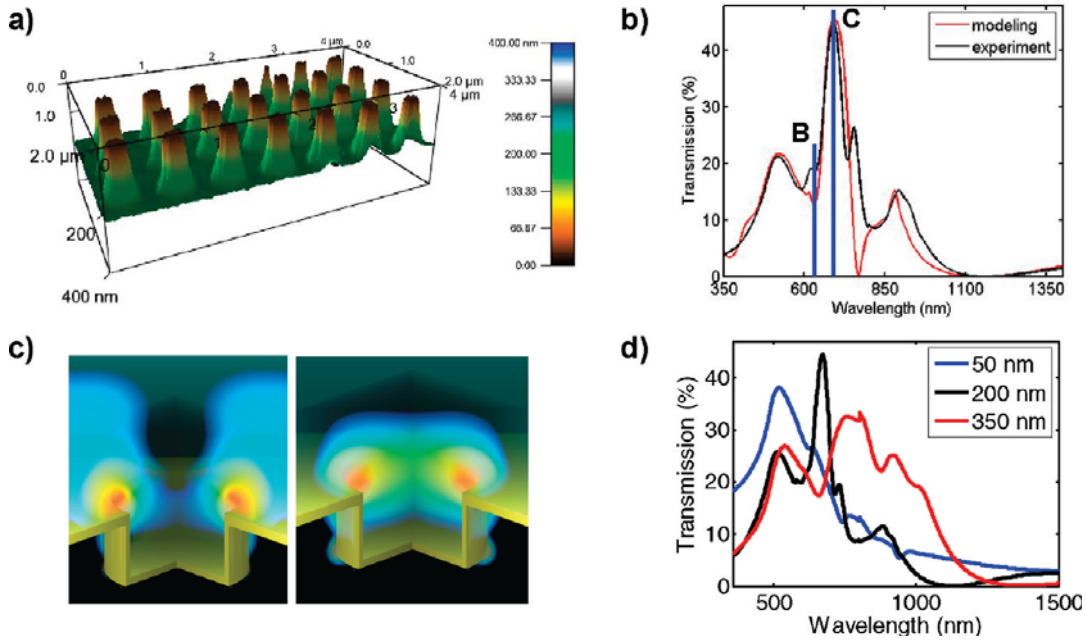

Figure 3. (a) Inverted 3D atomic force microscopy (AFM) image of the NOA-based plasmonic crystal nanostructures fabricated using the SOG master (~328 nm hole diameter, ~200 nm hole depth, ~560 nm hole spacing). (b) Experimental transmission spectrum (black) for full 3D NOA-based plasmonic crystal depicted in panel a and FDTD calculated transmission spectrum (red). (c) FDTD calculated electric field plots corresponding to optical features marked B (633 nm) and C (689 nm) in panel b. (d) Normal-incidence transmission spectra of NOA plasmonic crystals fabricated using SOG masters with different relief depths while maintaining other design parameters (hole diameter, periodicity, and gold thicknesses) constant.

and computationally through FDTD modeling are shown in Figure 3b. As in earlier work, the optical features of this system can be assigned to localized surface plasmon resonances (LSPRs), Bloch wave surface plasmon polaritions (BW-SPPs), and Wood's anomalies (WAs) or a combination of these features, as well as the background gold absorption around 500 nm.[29] The electric fields supported at wavelengths of 633 nm (B) and 689 nm (C) were calculated using the FDTD method and are presented in Figure 3c; the corresponding wavelengths are also indicated on the transmission spectra in Figure 3b. These plots reveal a high localization of the electric field around the rim of the nanohole at these wavelengths.

Additional SOG masters were fabricated with relief depths of 50 and 350 nm while keeping the other design parameters (*e.g.,* nanohole diameter and periodicity) constant by controlling the spin coating time as the initial SOG film was applied to the glass slide (Supporting Information, Figure SI2 presents AFM characterizations of these different relief depths). It is important to emphasize that these variable-depth SOG-based plasmonic crystals were all produced using a single elastomeric stamp; the relief depth of the original stamp was ~400 nm. NOA-based plasmonic crystals were replicated from these different SOG masters with relief depths of 50, 200, and 350 nm, and their transmission spectra compared (Figure 3d). These spectra clearly show shifts in the transmission that broadly span visible wavelengths as the nanohole depths increase, demonstrating an ability to tune the optical response of the plasmonic crystal during the SOG embossing that otherwise would have required the fabrication of separate photolithographic masters. This in turn should provide a means to reduce both the cost and time required for nanofabricating precision subwavelength optics.

The broader capacities that exist to tailor the optical properties of nanoimprinted plasmonic crystals between visible and near-infrared wavelengths is illustrated by the data presented in Supporting Information, Figure SI3a. The strongest transmission peak in the spectrum of a quasi 3D[27,52] plasmonic crystal system occurs at ~1200 nm; in the quasi-3D design, gold deposition *via* electron-beam evaporation coats the top surface of the device as well as the bottom of the nanoholes with little or no coverage on the nanohole sidewalls. This response shifts to ~900 nm in a full 3D[29] plasmonic crystal system, where gold deposition *via* sputtering results in the metal film coating the top surface and nanohole bottoms as well as on the nanohole sidewalls. Most strikingly, though, is the fact that the wavelength of the strongest peak can be further shifted (to ~700 nm) in the new design by simply optimizing the nanostructure relief depth using the control capabilities that accompany the use of embossed SOG nanostructures as replication masters.

More precise tuning of the optical response can be achieved using a combination of these techniques, and FDTD-based electrodynamics calculations can be

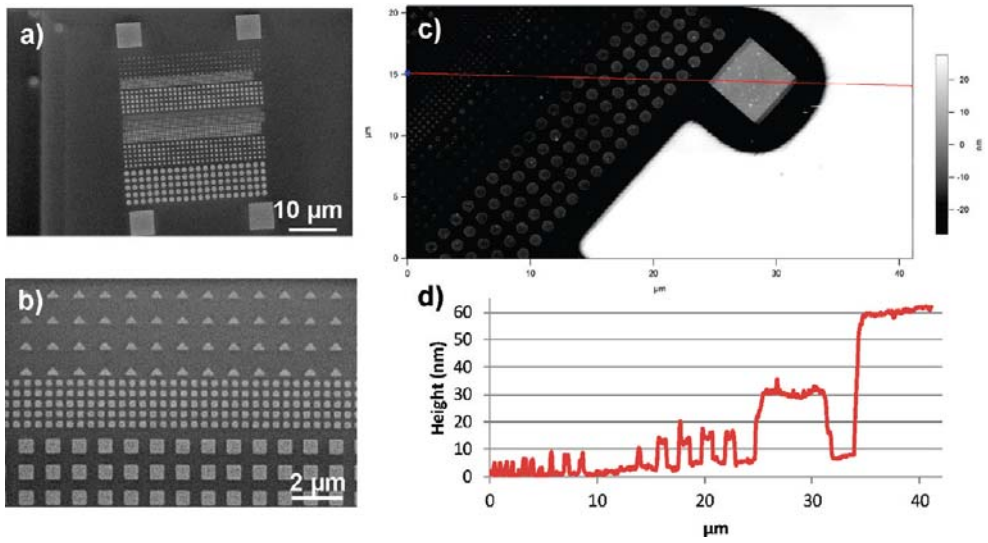

Figure 4. SEM images of nanostructures fabricated in PMMA layers *via* E-beam lithography with different shapes and sizes. (a) Large area top view and (b) high magnification view. (c) AFM image of the nanostructures embossed in SOG films using E-beam lithographic nanostructures as the replication master. (d) Structural profile following the red line in panel c across the nanostructures.

employed as a powerful tool for rationally tailoring *in silico* the plasmonic crystal dimensions for a specific application. For example, the results of a set of FDTD calculations are presented in Supporting Information, Figure SI3b, where the relief depth of the plasmonic nanohole array was varied between 50 and 600 nm. The red curve shows that the peak transmission wavelength of the plasmonic crystal can be tuned between 640 and 760 nm by adjusting the relief depth alone, with additional changes expected if the gold layer thicknesses or deposition characteristics are also changed. The calculated absolute transmittance at the peak transmission wavelength is plotted in black, and these two curves taken together show that although the peak transmission wavelength does not change monotonically in the relief depth range considered, different absolute transmittances can be realized at a single peak wavelength by targeting different relief depths. Theoretical computations can thus provide guidance in choosing the appropriate plasmonic crystal parameters for a particular application, and molding the device in spin-on-glass provides fabrication flexibility that previously has been unavailable.

Molecular-Scale Nanoimprinting Resolution Using SOG. As a demonstration of the replication resolution capable using SOG as an embossing medium, nanostructures with feature sizes between 5 and 200 nm were patterned by electron beam (E-beam) lithography (Figure 4a,b) and replicated in SOG. The E-beam lithography nanostructures were replicated as a composite h-PDMS/s-PDMS stamp, which was used in turn to transfer the E-beam patterns to an SOG film. The AFM data shown in Figure 4c displays a typical realized replication of a variety of E-beam lithographic structures in SOG, ones with different sizes and shapes. The relief depths of the replicated E-beam lithography structures vary from ~1 to ~50 nm as shown in the AFM line cut in Figure 4d; variations in the nanostructure heights follow those of the original E-beam lithographic masters.

Molecular scale molding experiments were performed using masters made of single-walled carbon nanotubes (SWNTs) grown on SiO_2/Si substrates. The h-PDMS/s-PDMS stamps were generated by casting and curing the elastomer against these SWNT masters and were subsequently used to emboss the SOG sol. The SWNT structures can be replicated on SOG films and are clearly distinguished from the unpatterned areas (Supporting Information, Figure SI4). The relief depth of the replicated SWNT structures could not be determined precisely, however, as the roughness of the SOG film at these dimensions is similar to the feature sizes of the master.

Chemical Stability of SOG-Based Plasmonic Nanostructures. The fully cured embossed SOG substrate is a glass-like inorganic film and is stable in common organic solvents. Piranha solution (highly oxidizing mixtures of concentrated sulfuric acid and hydrogen peroxide) and gold etchant are compatible with the SOG-embossed nanostructures, and these solutions have been used to aggressively clean the SOG plasmonic crystals by removing polymeric debris and stripping the metal layer. SEM images in Supporting Information, Figure SI5a compare the surface structures of one typical embossed SOG nanostructure before and after soaking in piranha solution over 24 h, and no changes were observed in the surface of the SOG nanostructures after cleaning. AFM measurements of the plasmonic crystal before and after piranha cleaning under the same conditions are presented in Supporting Information, Figure SI5b and show that the vertical profiles of

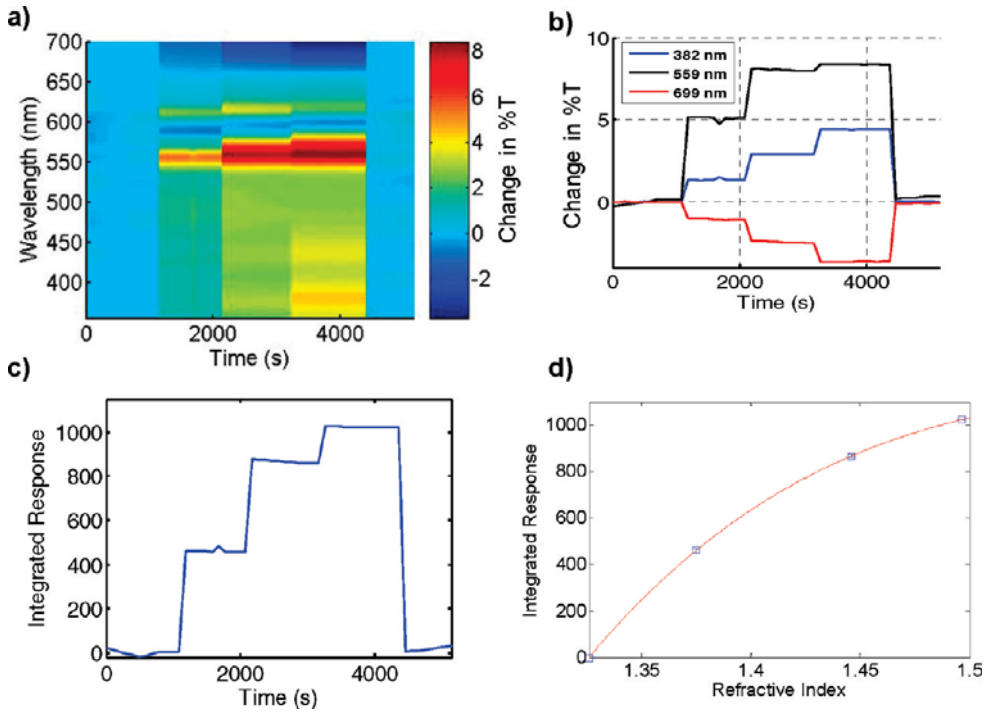

Figure 5. Multispectral analysis of organic solvent refractive index sensing using full 3D SOG plasmonic crystals with 35 nm thick gold films. (a) Color contour plot of the changes in transmission (*T*) with respect to the initial *T* at time *t* = 0 as a function of wavelength and time as solutions of increasing refractive index (*n*) are injected into the flow cell (the injection sequence is methanol (*n* = 1.326), 1-propanol (*n* = 1.384), chloroform (*n* = 1.445), and toluene (*n* = 1.496), and methanol). (b) Change in *T* at selected wavelengths as a function of time during the injection sequence. (c) Integrated multispectral plasmonic response as a function of time corresponding to the injection sequence described in panel a. (d) Integrated responses of the plasmonic crystal as a function of the refractive index of the organic solvent with a regression line corresponding to a cubic polynomial fit of the data included as a guide to the eye. Error bars representing the standard deviation of the measurement are included in the figure but are of the order of the size of the data symbols.

the relief structures also remain unaffected. These results clearly demonstrate that the SOG nanostructure is robust enough in piranha solution to withstand the regeneration treatment. Supporting Information, Figure SI5c displays the normal-incidence transmission spectra of NOA plasmonic crystals fabricated using a SOG master before and after piranha cleaning. The spectra are taken from arrays with periodicities of ~580 nm and ~740 nm. The transmission spectra of NOA plasmonic crystals replicated after the piranha cleaning are consistent with those collected from NOA crystals replicated from the SOG master before the piranha cleaning. The durability of the SOG nanostructures themselves and the consistency in the optical responses of the replicated NOA plasmonic crystals are convincing arguments for the application of these SOG-based nanostructures as masters for the replication of plasmonic nanostructures with high precision.

Refractive Index Sensing in Organic Solvent Environments. Substituting a SOG material for photocurable polymers can markedly extend the scope of applications for plasmonic crystal-based sensing. For example, the inorganic nature of the SOG materials extends the capacities of plasmonic platforms for organic sensing applications, which is otherwise impossible using polymer-supported plasmonic crystals due to the instability of these substrate materials in organic solvents. As a demonstration, refractive index sensitivity measurements were made by flowing different organic solvents (methanol, 1-propanol, chloroform, and toluene) over the plasmonic crystal surface; the results are presented in Figure 5. The difference spectra over a wavelength range of 355−700 nm analyzed using a multispectral sensitivity method we described in earlier work[27,29] are given in Figure 5a. This wavelength range was chosen to avoid the absorption of near-infrared light by the organic solvents themselves. Spectral changes at specific wavelengths are provided in Figure 5b, further demonstrating the wavelength-specific transmission behaviors of plasmonic crystal-based SPR sensors.[27,29] The integrated responses of the plasmonic crystal to changes in the organic solvent environment were calculated using a previously described multispectral analysis method that weights integrated absolute intensity changes.[26,27,29] The results of this analysis are presented in Figure 5c, where one notes clear and progressively varying step responses upon introduction of the different solvents. The integrated response change as a function of the refractive index of the organic solvent is shown in Figure 5d; the change noted in the integrated response of a SOG plasmonic crystal is approximately linear over a broad range of

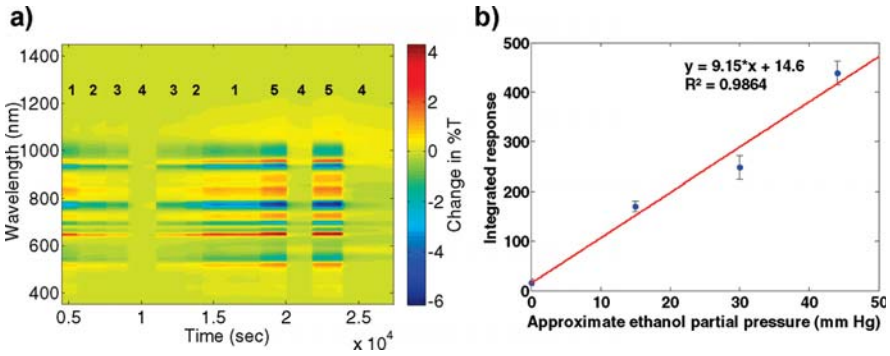

Figure 6. Multispectral analysis of organic vapor sensing using full 3D SOG plasmonic crystals with ~35 nm thick gold films and ~50 nm thick porous TiO_2 layer formed on top of gold film using glancing angle E-beam deposition. (a) Color contour plot of the changes in transmission with respect to the initial transmission at time $t = 0$ as a function of wavelength and time as ethanol/argon gas mixtures with different concentrations of ethanol are injected into the flow cell. The numbers overlaid on the plot correspond to the following gas compositions: (1) ~44 mmHg ethanol vapor in argon, (2) ~30 mmHg ethanol vapor in argon, (3) ~15 mmHg ethanol vapor in argon, (4) argon, and (5) ~59 mmHg ethanol vapor in argon. (b) Calibration curve for the integrated response as a function of ethanol partial pressures between 0–44 mmHg.

refractive indices. In control experiments, these same solvents destroyed plasmonic crystals embossed in polyurethane (NOA). The improved chemical stability of the embossed SOG plasmonic crystals thus supports prospects for their use in more aggressive chemical or nonaqueous environments for refractive index based sensing and imaging.

Refractive Index Sensing of Organic Vapors. The high analytical sensitivity of embossed SOG plasmonic crystals was demonstrated through an organic vapor sensing experiment using mixtures of argon and ethanol vapor. A gas mixing device was designed to obtain dry mixtures of different gases with proportions set by partial pressure measurements. The SOG plasmonic crystal was exposed to different ethanol vapor concentrations in a Teflon flow cell, and the normal incidence transmission spectra collected as a function of time. To take advantage of the effective sensing volume of the plasmonic crystal, a porous TiO_2 film was deposited on it using glancing-angle E-beam deposition[61,62] to increase the surface area and sorptive affinity of the plasmonic crystal for the organic vapor. The multispectral analysis presented in Figure 6a shows that the refractive index change associated with changes in ethanol vapor concentration are readily detected by this modified SOG plasmonic crystal. (A graphical representation of the ethanol vapor concentrations used during the experiment is presented in Supporting Information, Figure SI6a.) This multispectral analysis coupled with the single wavelength plots in Figure SI6b show that the transmission difference measured at specific single wavelengths is a direct function of the ethanol partial pressure and returns to the initial value when the gas mixture returns to the initial ethanol concentration (the minor deviations of the transmission from the initial value are likely the result of imprecise partial pressure control using this home-built setup). The integrated response of this SOG plasmonic crystal to changes in ethanol partial pressure is approximately linear at partial pressures ranging from 0 to 44 mmHg, a representative calibration curve for which is presented in Figure 6b. On the basis of this calibration curve, a conservative estimate of the limit of detection for the sensor with the current acquisition parameters is an ethanol partial pressure in argon of ~2.4 mmHg. This is not a hard limit as signal averaging and modification of other instrumental (*i.e.*, nonplasmonic crystal) components would naturally extend this limit. These experiments support the capacity of SOG plasmonic crystals for organic sensing involving small refractive index variations and suggest the possibility of their use as gas/vapor sensors.

Surface-Enhanced Raman Spectroscopy Using SOG Plasmonic Crystals. SOG plasmonic crystals formed by soft nanoimprint lithography also provide a low-cost and well-controlled substrate for surface-enhanced Raman spectroscopy (SERS).[30] The inorganic nature of the SOG embossed structure is more stable at high temperatures compared to photocurable organic materials. For instance, the fabrication of SOG plasmonic crystals involves thermally annealing the structures at 450 °C. The thermal durability of the embossed surface features of the SOG plasmonic crystal at this temperature suggests they may outperform conventional organic-based plasmonic crystals under the high power lasers used in Raman microscopy. We find, for example, that plasmonic crystals fabricated using NOA and SU8 photoresist are grossly distorted by local heating when irradiated with a laser at 785 nm with a reasonably high power of ~50 mW (Supporting Information, Figure SI7a–d). The corresponding plasmonic nanostructures embossed in SOG (Figure SI7e,f) are not impacted by exposure to the laser in this way (although some annealing of the Au film due to the local heating at this limiting power is noted).

As a comparison, quasi-3D plasmonic crystals (an effective SERS design)[30] were molded using SOG, NOA, and SU8 and a benzenethiol self-assembled monolayer formed subsequently on each under identical

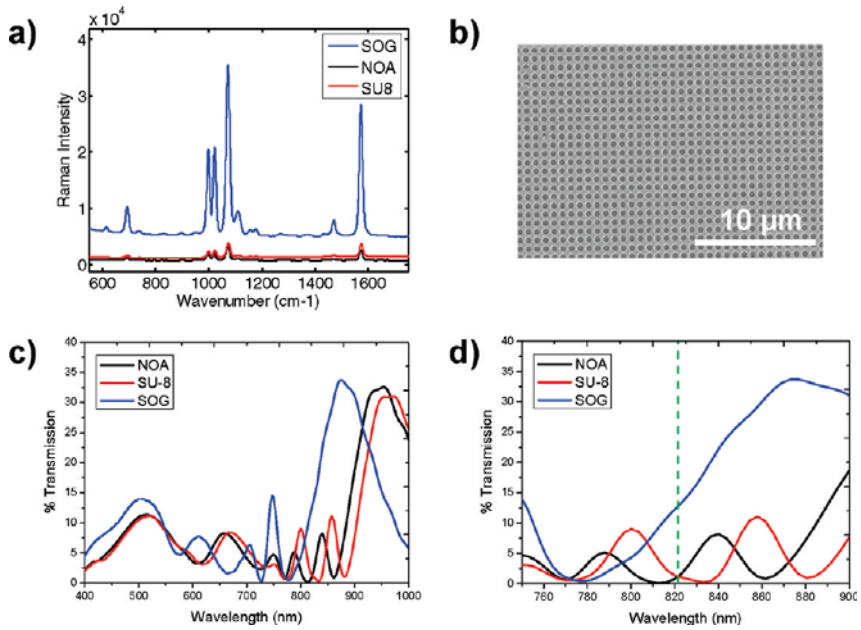

Figure 7. (a) SERS spectra of benzenethiol adsorbed onto three different embossed SERS substrates (molded in SOG, NOA, and SU8) measured with laser power of ~0.5 mW. (b) SEM image of the SOG molded plasmonic crystal after exposure to a laser power of ~0.5 mW, which shows that the SOG structure is not damaged by the laser exposure. (c) Simulated transmission spectra for NOA, SU-8, and SOG molded plasmonic crystals with dimensions similar to the nanostructures used to collect the Raman spectra in (a): 440 nm hole diameters, 740 nm periodicities, 48 nm Au film on the top surface, and 40 nm Au discs in the bottom of the nanoholes. (d) Magnified view of the spectra shown in panel c with a green dotted line at 821 nm.

experimental conditions. Figure 7a displays the surface-enhanced Raman spectrum of benzenethiol collected from the SOG, NOA, and SU8-based plasmonic crystals and clearly demonstrates a larger Raman signal—approximately 10-fold enhancement—from the SOG-based nanostructures. An SEM image of the exposed SOG molded plasmonic crystal area after the SERS measurement is shown in Figure 7b. No visible damage or distortion of the nanostructures or the gold film is noted for the power used in this measurement.

Previous work has shown a correlation between the SERS enhancement of a plasmonic substrate and its optical transmission (and thus the underlying plasmonic properties) at a wavelength halfway between the laser excitation wavelength and the Raman scattered wavelength, with larger Raman enhancements observed for systems displaying greater transmission at this halfway point wavelength.[30,58] In this study, this corresponds to a halfway point of 821 nm for a laser excitation of 785 nm and a Raman scattered wavelength of 857 nm (which corresponds to the Raman peak at ~1060 cm^{-1}). FDTD simulated transmission spectra of NOA, SU-8, and SOG plasmonic crystals with feature dimensions corresponding to the samples used experimentally are presented in Figure 7c. Figure 7d shows a magnified view of the spectra in Figure 7c with a green dotted line indicating a wavelength of 821 nm. The percent transmission value of the NOA and SU-8 based plasmonic crystals at this wavelength are very similar while the transmission of the SOG plasmonic crystal is markedly higher; these results qualitatively mirror the relative Raman enhancements measured for benzenethiol on these systems and are in agreement with the findings reported in previously published work.

We should note that the higher thermal stability of the SOG substrate is expected to delay the onset of thermal deformation of the nanostructures, allowing as a result longer effective SERS signal collection times. While SERS signals were collected using the same power and duration for all three substrates, it is possible that thermal damage in the organic substrates might adversely impact the Raman enhancements in ways that complicate precise quantitative comparisons. Thus, the larger Raman enhancements observed for the SOG-based plasmonic crystals likely result from a convolution of factors: differences in the optical and plasmonic properties of the substrates themselves (as seen in the transmission spectra) coupled with increased thermal stability. However this might be, the end result is that the inorganic plasmonic crystal system outperforms its organic counterparts by nearly an order of magnitude.

We carried out FDTD calculations to develop a better understanding of a specific feature (the "half-wavelength" of merit) that serves to distinguish SERS optics fabricated using a polymer such as NOA from ones with an equivalent design rule but supported on an embossed SOG substrate. These calculated transmission spectra presented in Figure 7c reveal the importance of the refractive index of the embossing material itself on the optical transmission properties that result at the previously discussed half-wavelength

of merit (and thus the supported plasmon modes) that result. These calculations show that the observed resonances in the SOG-based plasmonic crystal are shifted to shorter wavelengths as compared to the organic systems examined, with intensity differences at the half-wavelength of 821 nm of sufficient magnitude to impact the SERS enhancements. These effects are shown by these calculations to be due to refractive index differences in the substrate itself. The use of spin-on-glass with its marked refractive index contrast ($n \approx 1.38$) compared to the polymer systems ($n \approx 1.5-1.6$) previously explored provides another lever by which the properties of these plasmonic crystals or other plasmonic substrates can be tuned to specific wavelength regions that otherwise may be inaccessible using existing design rules and molding materials.

CONCLUSIONS

We have described the adaptation of an inorganic spin-on glass (SOG) material capable of embossing at molecular scale resolutions for the fabrication of plasmonic crystal nanostructures. These SOG nanostructures are shown to be stable in a wide range of chemical environments and have been used as masters for the replication of additional plasmonic crystals. The fabrication procedure for these plasmonic crystals can be adjusted to tune the resultant relief depths of the replicated nanostructures, and this versatility combined with the optical properties of the SOG itself provide powerful parameters for tuning the optical properties of the plasmonic device. The use of SOG as a molding material for nanohole arrays further extends the utility of these plasmonic crystals as stable, low cost platforms for high-performance liquid-phase and vapor-phase sensing through surface plasmon resonance and surface-enhanced Raman spectroscopy measurements. Chemical selectivity and specificity can be engineered into the sensor by functionalizing the plasmonic crystal surface with analyte-specific recognition mechanisms (such as DNA aptamers or antibodies).[26,27,63,64] The material properties and the processing controls demonstrated here are powerful enablers for adapting these plasmonic crystals to meet the continually evolving demand for inexpensive, yet high-performance, sensing devices.

MATERIALS AND METHODS

Materials. All reagents were used as received without further purification. Spin on glass (SOG) (product number 314) was purchased from Honeywell. Polydimethylsiloxane (soft PDMS (s-PDMS), Dow Corning, Sylgard 184) was obtained from Ellsworth Adhesives and prepared according to the manufacturer's directions. Components for hard PDMS (h-PDMS): poly(25−30% methylhydrosiloxane)-(dimethylsiloxane) (HMS-301), (1,3,5,7-tetravinyl-1,3,5,7-tetramethylcyclotetrasiloxane) (SIT-7900), poly-(7−8% vinylmethylsiloxane)-(dimethylsiloxane) (VDT-731), and platinum-divinyltetramethyldisiloxane (SIP-6831.1) were purchased from Gelest. Fluorinated silane (tridecafluoro-1,1,2,2-tetrahydrooctyl)trichlorosilane (TDFOCS) was purchased from Gelest. Photocurable polyurethane (PU, NOA73) was purchased from Norland Products. Negative photoresist SU-8 was purchased from MicroChem. Benzenethiol (BT) (99.99%) was purchased from Aldrich. Gold etchant TFA was purchased from Transene Company, Inc. Deionized (DI) water (18 MΩ) was generated using a Millipore Milli-Q Academic A-10 system. Polymethyl methacrylate (PMMA A2) used for E-beam lithography was purchased from MicroChem Corporation. Piranha solution, a 7:3 mixture of H_2SO_4/H_2O_2, was used to remove organic contamination from the SOG molds. **Caution:** The use of piranha solution is highly dangerous and should be handled using appropriate personal protective equipment and proper safety procedures.

Fabrication of SOG Plasmonic Crystals. SOG material, designed as an interlevel dielectric material in the semiconductor industry, is used here to produce stable inorganic plasmonic crystals. SOG was filtered through 0.22 and 0.02 μm syringe filters before spin-casting (700 rpm for 10 s) to form a thin SOG layer (~1 μm thick) on top of a glass slide. The SOG soft gel was embossed by conformal contact with a composite h-PDMS/s-PDMS stamp consisting of nanohole array relief structures.[21,22,27,29,52] The sample was soft baked at 110 °C for 3 min after which the PDMS stamp was carefully removed. The embossed SOG film was further cured at 200 °C for 5 min and annealed at 450 °C under nitrogen for 1 h. An ~5 nm tin(IV) oxide film as an adhesion layer followed by a gold film were deposited on the embossed SOG structure by sputter deposition in 5 mTorr argon (AJA International). For organic vapor sensing experiments, a thin layer of titanium oxide with thickness about 50 nm was deposited on the surface of SOG plasmonic crystals following the Au deposition by glancing angle electron beam evaporation.[62]

Fabrication of Plasmonic Crystals Using SOG Masters. The fabrication procedure for plasmonic crystals using SOG embossed nanostructures as masters is similar to the procedure previously described.[28−30] A monolayer of fluorinated silanes was formed on the SOG embossed nanostructure to aid the separation of the SOG surface from the composite h-PDMS/s-PDMS stamp.[52] The PDMS stamp was then used to emboss photocurable organic prepolymers or SOG sol to generate new plasmonic nanostructures.

E-beam Lithography for Writing Nanostructures. A Raith e-Line electron beam lithography system and nanoengineering workstation was used to design and write nanostructures. Minimum line widths less than 20 nm, stitching accuracy around 40 nm, and overlay accuracy around 40 nm are possible using this system. The operation conditions used for writing PMMA layers with thicknesses of ~100 nm were as follows: voltage, 10 or 20 KV; aperture, 10 μm, 20 μm, or 30 μm; working distance, 10 mm. PMMA A2 was spin-coated onto a silicon wafer (4000 rpm for 40 s) with a resulting thickness around 100 nm. The sample was partially cured at 100 °C for 1 min and then cured at 180 °C for 2 min. After electron beam exposure using the Raith e-Line system, the PMMA layer was developed using a 1:3 solution of methyl isobutyl ketone (MIBK)/isopropanol (IPA) for 40 − 80 s, rinsed with IPA, and dried with nitrogen.

Molecular Scale Molding. Randomly aligned individual single-walled carbon nanotubes (SWNTs) with diameters between 0.6 and 3.0 nm and surface coverage of ~1−10 tubes/μm^2 were grown on SiO_2/Si wafers using chemical vapor deposition according to procedures described previously.[21,65] These SWNT structures were used as a master to fabricate elastomeric molds for the soft nanoimprinting of SOG materials with molecular scale features. A monolayer of fluorinated silanes on the SWNT masters is necessary to aid in the separation of the SWNT master and the composite PDMS stamp.[52]

Transmission-Mode Spectroscopy. Transmission spectra of SOG plasmonic crystals were measured using a Varian 5G UV–vis–NIR spectrophotometer operating in normal incidence transmission mode without temperature control. A flow cell was mounted on top of the plasmonic crystal and organic solvents with increasing refractive indexes were injected into the flow cell with a syringe pump (Harvard Apparatus) at a flow rate of 0.1 mL/min. Transmission spectra over a wavelength range of 355–700 nm were collected during the process to monitor the changes in multiple plasmonic responses to those of the surrounding dielectric environment.

FDTD Calculations. Finite-difference time-domain calculations[66–70] were used to model the normal incidence transmission spectra and electromagnetic field distributions of NOA, SU-8, and SOG-based plasmonic crystals from a SOG master in air. The unit cell geometry defines an infinite square array of nanostructured gold film parallel to the x–y plane with semi-infinite NOA material on the bottom side and air on the top side. The unit cell involved $N_x \times N_y \times N_z = 142 \times 142 \times 750$ total grid points. Propagations in the unit cell were carried out for 150 fs. Uniaxial perfectly matching layers were applied on both sides of the z grid to avoid artificial reflection errors from domain boundaries. Appropriate periodic boundary conditions were used to define the edge of the x–y plane consistent with the geometry of the infinite square array. The frequency-dependent gold permittivity was described by a Drude plus two-pole Lorentzian model over a wavelength range of 350–1500 nm. The dielectric constants of NOA, SU-8, SOG, water, and air were taken to be 2.43, 2.56, 1.90, 1.78, and 1.00, respectively.

SERS Measurements. Surface-enhanced Raman spectroscopy measurements were conducted using a SENTERRA dispersive Raman microscope (Bruker Optics) with a 785 nm excitation laser and an excitation power of ~2.7 mW. The Raman spectra were collected over a Raman shift range of 440–1800 cm^{-1}. Gold (50 nm) was deposited onto the surface of the plasmonic crystals *via* electron beam evaporation. A self-assembled monolayer of benzenethiol was formed on top of the plasmonic crystals by immersing them in a 15 mM benzenethiol ethanol solution overnight, rinsing thoroughly with ethanol, and drying with N_2.

Acknowledgment. This material is based upon work supported as part of the Light-Material Interactions in Energy Conversion, an Energy Frontier Research Center funded by the U.S. Department of Energy, Office of Science, Office of Basic Energy Sciences under prime contract DE-SC0001293 to the California Institute of Technology *via* subaward 67N-1087758 to the University of Illinois. The authors gratefully acknowledge use of the Frederick Seitz Materials Research Laboratory Central Facilities at the University of Illinois, including the Center for Microanalysis of Materials, supported by the U.S. Department of Energy, Basic Energy Science, Materials Science and Engineering Division under Award No. DE-FG02-07ER46471. The work at the Center for Nanoscale Materials at Argonne National Laboratory was supported by the U.S. Department of Energy, Office of Science, Office of Basic Energy Sciences, under Contract No. DE-AC02-06CH11357. The authors also gratefully acknowledge the use of the Turing cluster maintained and operated by the Computational Science and Engineering Program at the University of Illinois.

Supporting Information Available: SEM micrographs of SOG particulates, AFM plots and transmission spectra (both experimental and simulated) for plasmonic nanostructures with varying relief depths, SEM and AFM characterization of e-beam lithography nanostructure and carbon nanotube replication in SOG; SEM, AFM, and spectral characterization of SOG-based nanostructures following treatment with piranha solution. This material is available free of charge *via* the Internet at http://pubs.acs.org.

REFERENCES AND NOTES

1. Stewart, M. E.; Motala, M. J.; Yao, J.; Thompson, L. B.; Nuzzo, R. G. Unconventional Methods for Forming Nanopatterns. *Proc. Inst. Mech. Eng. Part N, J. Nanoeng. Nanosyst.* **2007**, *220*, 81–138.
2. Xia, Y. N.; Rogers, J. A.; Paul, K. E.; Whitesides, G. M. Unconventional Methods for Fabricating and Patterning Nanostructures. *Chem. Rev.* **1999**, *99*, 1823–1848.
3. Gates, B. D.; Xu, Q. B.; Stewart, M.; Ryan, D.; Willson, C. G.; Whitesides, G. M. New Approaches to Nanofabrication: Molding, Printing, and Other Techniques. *Chem. Rev.* **2005**, *105*, 1171–1196.
4. Love, J. C.; Estroff, L. A.; Kriebel, J. K.; Nuzzo, R. G.; Whitesides, G. M. Self-Assembled Monolayers of Thiolates on Metals as a Form of Nanotechnology. *Chem. Rev.* **2005**, *105*, 1103–1169.
5. Rosa, L. G.; Liang, J. Atomic Force Microscope Nanolithography: Dip-Pen, Nanoshaving, Nanografting, Tapping Mode, Electrochemical and Thermal Nanolithography. *J. Phys.-Condens. Matter* **2009**, *21*, 483001.
6. Salaita, K.; Wang, Y. H.; Mirkin, C. A. Applications of Dip-Pen Nanolithography. *Nat. Nanotechnol.* **2007**, *2*, 145–155.
7. Koh, S. J. Strategies for Controlled Placement of Nanoscale Building Blocks. *Nanoscale Res. Lett.* **2007**, *2*, 519–545.
8. Kim, J. K.; Yang, S. Y.; Lee, Y.; Kim, Y. Functional Nanomaterials Based on Block Copolymer Self-Assembly. *Prog. Polym. Sci.* **2010**, *35*, 1325–1349.
9. Suh, K. Y.; Park, M. C.; Kim, P. Capillary Force Lithography: A Versatile Tool for Structured Biomaterials Interface Towards Cell and Tissue Engineering. *Adv. Funct. Mater.* **2009**, *19*, 2699–2712.
10. Zhang, G.; Wang, D. Y. Colloidal Lithography-the Art of Nanochemical Patterning. *Chem.-Asian J.* **2009**, *4*, 236–245.
11. Zhang, X.; Whitney, A. V.; Zhao, J.; Hicks, E. M.; Van Duyne, R. P. Advances in Contemporary Nanosphere Lithographic Techniques. *J. Nanosci. Nanotechnol.* **2006**, *6*, 1920–1934.
12. Zhang, X.; Yonzon, C.; Van Duyne, R. P. Nanosphere Lithography Fabricated Plasmonic Materials and Their Applications. *J. Mater. Res.* **2006**, *21*, 1083–1092.
13. Henzie, J.; Barton, J. E.; Stender, C. L.; Odom, T. W. Large-Area Nanoscale Patterning: Chemistry Meets Fabrication. *Acc. Chem. Res.* **2006**, *39*, 249–257.
14. Henzie, J.; Lee, J.; Lee, M. H.; Hasan, W.; Odom, T. W. Nanofabrication of Plasmonic Structures. *Annu. Rev. Phys. Chem.* **2009**, *60*, 147–165.
15. Bailey, T. C.; Johnson, S. C.; Sreenivasan, S. V.; Ekerdt, J. G.; Willson, C. G.; Resnick, D. J. Step and Flash Imprint Lithography: An Efficient Nanoscale Printing Technology. *J. Photopolym. Sci. Technol.* **2002**, *15*, 481–486.
16. Colburn, M.; Grot, A.; Amistoso, M.; Choi, B. J.; Bailey, T.; Ekerdt, J.; Sreenivasan, S. V.; Hollenhorst, J.; Willson, C. G. In Step and Flash Imprint Lithography for Sub-100 Nm Patterning. Emerging Lithographic Technologies IV, Febrary 28, 2000–March 1, 2000, Santa Clara, CA, USA; Society of Photo-Optical Instrumentation Engineers: Santa Clara, CA, USA, 2000; pp 453–457.
17. Qin, D.; Xia, Y. N.; Whitesides, G. M. Soft Lithography for Micro- and Nanoscale Patterning. *Nat. Protoc.* **2010**, *5*, 491–502.
18. Randolph, S. J.; Fowlkes, J. D.; Rack, P. D. Focused, Nanoscale Electron-Beam-Induced Deposition and Etching. *Crit. Rev. Solid State Mater. Sci.* **2006**, *31*, 55–89.
19. Tseng, A. A. Recent Developments in Micromilling Using Focused Ion Beam Technology. *J. Micromech. Microeng.* **2004**, *14*, R15–R34.
20. Xia, Y.; Whitesides, G. M. Soft Lithography. *Angew. Chem., Int. Ed.* **1998**, *37*, 550–575.
21. Hua, F.; Sun, Y.; Gaur, A.; Meitl, M. A.; Bilhaut, L.; Rotkina, L.; Wang, J.; Geil, P.; Shim, M.; Rogers, J. A. Polymer Imprint Lithography with Molecular-Scale Resolution. *Nano Lett.* **2004**, *4*, 2467–2471.
22. Truong, T. T.; Lin, R.; Jeon, S.; Lee, H. H.; Maria, J.; Gaur, A.; Hua, F.; Meinel, I.; Rogers, J. A. Soft Lithography Using Acryloxy Perfluoropolyether Composite Stamps. *Langmuir* **2007**, *23*, 2898–2905.
23. Piner, R. D.; Zhu, J. Z.; Xu, F.; Hong, S.; Mirkin, C. A. "Dip-Pen" Nanolithography. *Science* **1999**, *283*, 661–663.
24. Loo, Y.-L.; Lang, D. V.; Rogers, J. A.; Hsu, J. W. P. Electrical Contacts to Molecular Layers by Nanotransfer Printing. *Nano Lett.* **2003**, *3*, 913–917.

25. Loo, Y.-L.; Willett, R. L.; Baldwin, K. W.; Rogers, J. A. Interfacial Chemistries for Nanoscale Transfer Printing. *J. Am. Chem. Soc.* **2002**, *124*, 7654–7655.
26. Stewart, M. E.; Anderton, C. R.; Thompson, L. B.; Maria, J.; Gray, S. K.; Rogers, J. A.; Nuzzo, R. G. Nanostructured Plasmonic Sensors. *Chem. Rev.* **2008**, *108*, 494–521.
27. Stewart, M. E.; Mack, N. H.; Malyarchuk, V.; Soares, J. A. N. T.; Lee, T.-W.; Gray, S. K.; Nuzzo, R. G.; Rogers, J. A. Quantitative Multispectral Biosensing and 1D Imaging Using Quasi-3D Plasmonic Crystals. *Proc. Natl. Acad. Sci. U.S.A.* **2006**, *103*, 17143–17148.
28. Yao, J.; Le, A.-P.; Gray, S. K.; Moore, J. S.; Rogers, J. A.; Nuzzo, R. G. Functional Nanostructured Plasmonic Materials. *Adv. Mater.* **2010**, *22*, 1102–1110.
29. Yao, J.; Stewart, M. E.; Maria, J.; Lee, T.-W.; Gray, S. K.; Rogers, J. A.; Nuzzo, R. G. Seeing Molecules by Eye: Surface Plasmon Resonance Imaging at Visible Wavelengths with High Spatial Resolution and Submonolayer Sensitivity. *Angew. Chem., Int. Ed.* **2008**, *47*, 5013–5017.
30. Baca, A. J.; Truong, T. T.; Cambrea, L. R.; Montgomery, J. M.; Gray, S. K.; Abdula, D.; Banks, T. R.; Yao, J.; Nuzzo, R. G.; Rogers, J. A. Molded Plasmonic Crystals for Detecting and Spatially Imaging Surface Bound Species by Surface-Enhanced Raman Scattering. *Appl. Phys. Lett.* **2009**, *94*, 243109/1–243109/3.
31. Camden, J. P.; Dieringer, J.; Zhao, J.; Van Duyne, R. P. Controlled Plasmonic Nanostructures for Surface-Enhanced Spectroscopy and Sensing. *Acc. Chem. Res.* **2008**, *41*, 1653–1661.
32. Gordon, R.; Sinton, D.; Kavanagh, K. L.; Brolo, A. G. A New Generation of Sensors Based on Extraordinary Optical Transmission. *Acc. Chem. Res.* **2008**, *41*, 1049–1057.
33. Stuart, D. A.; Haes, A. J.; Yonzon, C. R.; Hicks, E. M.; Van Duyne, R. P. Biological Applications of Localised Surface Plasmonic Phenomenae. *IEE Proc. Nanobiotechnol.* **2005**, *152*, 13–22.
34. Willets, K. A.; Van Duyne, R. P. Localized Surface Plasmon Resonance Spectroscopy and Sensing. *Annu. Rev. Phys. Chem.* **2007**, *58*, 267–297.
35. Barnes, W. L. Fluorescence Near Interfaces: The Role of Photonic Mode Density. *J. Mod. Opt.* **1998**, *45*, 661–699.
36. Aslan, K.; Gryczynski, I.; Malicka, J.; Matveeva, E.; Lakowicz, J. R.; Geddes, C. D. Metal-Enhanced Fluorescence: An Emerging Tool in Biotechnology. *Curr. Opin. Biotechnol.* **2005**, *16*, 55–62.
37. Lakowicz, J. R. Radiative Decay Engineering 5: Metal-Enhanced Fluorescence and Plasmon Emission. *Anal. Biochem.* **2005**, *337*, 171–194.
38. Liebermann, T.; Knoll, W. Surface-Plasmon Field-Enhanced Fluorescence Spectroscopy. *Colloid Surf. A* **2000**, *171*, 115–130.
39. Ferry, V. E.; Sweatlock, L. A.; Pacifici, D.; Atwater, H. A. Plasmonic Nanostructure Design for Efficient Light Coupling into Solar Cells. *Nano Lett.* **2008**, *8*, 4391–4397.
40. Nakayama, K.; Tanabe, K.; Atwater, H. A. Plasmonic Nanoparticle Enhanced Light Absorption in GaAs Solar Cells. *Appl. Phys. Lett.* **2008**, *93*, 121904.
41. Pillai, S.; Catchpole, K. R.; Trupke, T.; Green, M. A. Surface Plasmon Enhanced Silicon Solar Cells. *J. Appl. Phys.* **2007**, *101*, 093105.
42. Stuart, H. R.; Hall, D. G. Island Size Effects in Nanoparticle-Enhanced Photodetectors. *Appl. Phys. Lett.* **1998**, *73*, 3815–3817.
43. Chang, C.-K.; Lin, D.-Z.; Yeh, C.-S.; Lee, C.-K.; Chang, Y.-C.; Lin, M.-W.; Yeh, J.-T.; Liu, J.-M. Experimental Analysis of Surface Plasmon Behavior in Metallic Circular Slits. *Appl. Phys. Lett.* **2007**, *90*, 061113/1–061113/3.
44. Dintinger, J.; Klein, S.; Ebbesen, T. W. Molecule-Surface Plasmon Interactions in Hole Arrays: Enhanced Absorption, Refractive Index Changes, and All-Optical Switching. *Adv. Mater.* **2006**, *18*, 1267–1270.
45. Grand, J.; Adam, P.-M.; Grimault, A.-S.; Vial, A.; de la Chapelle, M. L.; Bijeon, J.-L.; Kostcheev, S.; Royer, P. Optical Extinction Spectroscopy of Oblate, Prolate and Ellipsoid Shaped Gold Nanoparticles: Experiments and Theory. *Plasmonics* **2006**, *1*, 135–140.
46. Rechberger, W.; Hohenau, A.; Leitner, A.; Krenn, J. R.; Lamprecht, B.; Aussenegg, F. R. Optical Properties of Two Interacting Gold Nanoparticles. *Opt. Commun.* **2003**, *220*, 137–141.
47. Bozhevolnyi, S. I.; Volkov, V. S.; Devaux, E.; Laluet, J.-Y.; Ebbesen, T. W. Channel Plasmon Subwavelength Waveguide Components Including Interferometers and Ring Resonators. *Nature* **2006**, *440*, 508–511.
48. Przybilla, F.; Genet, C.; Ebbesen, T. W. Enhanced Transmission through Penrose Subwavelength Hole Arrays. *Appl. Phys. Lett.* **2006**, *89*, 121115.
49. Gao, H.; McMahon, J. M.; Lee, M. H.; Henzie, J.; Gray, S. K.; Schatz, G. C.; Odom, T. W. Rayleigh Anomaly-Surface Plasmon Polariton Resonances in Palladium and Gold Subwavelength Hole Arrays. *Opt. Express* **2009**, *17*, 2334.
50. Henzie, J.; Lee, M. H.; Odom, T. W. Multiscale Patterning of Plasmonic Metamaterials. *Nat. Nanotechnol.* **2007**, *2*, 549–554.
51. Kwak, E.-S.; Henzie, J.; Chang, S.-H.; Gray, S. K.; Schatz, G. C.; Odom, T. W. Surface Plasmon Standing Waves in Large-Area Subwavelength Hole Arrays. *Nano Lett.* **2005**, *5*, 1963–1967.
52. Malyarchuk, V.; Hua, F.; Mack, N. H.; Velasquez, V. T.; White, J. O.; Nuzzo, R. G.; Rogers, J. A. High Performance Plasmonic Crystal Sensor Formed by Soft Nanoimprint Lithography. *Opt Express* **2005**, *13*, 5669–5675.
53. Truong, T. T.; Maria, J.; Yao, J.; Stewart, M. E.; Lee, T.-W.; Gray, S. K.; Nuzzo, R. G.; Rogers, J. A. Nanopost Plasmonic Crystals. *Nanotechnol.* **2009**, *20*, 434011–1/434011−8.
54. Mack, N. H.; Wackerly, J. W.; Malyarchuk, V.; Rogers, J. A.; Moore, J. S.; Nuzzo, R. G. Optical Transduction of Chemical Forces. *Nano Lett.* **2007**, *7*, 733–737.
55. Jeanmaire, D. L.; Van Duyne, R. P. Surface Raman Spectroelectrochemistry Part I. Heterocyclic, Aromatic, and Aliphatic Amines Adsorbed on the Anodized Silver Electrode. *J. Electroanal. Chem.* **1977**, *84*, 1–20.
56. Albrecht, M. G.; Creighton, J. A. Anomalously Intense Raman Spectra of Pyridine at a Silver Electrode. *J. Am. Chem. Soc.* **1977**, *99*, 5215–5217.
57. Nie, S.; Emory, S. R. Probing Single Molecules and Single Nanoparticles by Surface-Enhanced Raman Scattering. *Science* **1997**, *275*, 1102–1106.
58. Haynes, C. L.; Van Duyne, R. P. Plasmon-Sampled Surface-Enhanced Raman Excitation Spectroscopy. *J. Phys. Chem. B* **2003**, *107*, 7426–7433.
59. Tao, A.; Kim, F.; Hess, C.; Goldberger, J.; He, R.; Sun, Y.; Xia, Y.; Yang, P. Langmuir−Blodgett Silver Nanowire Monolayers for Molecular Sensing Using Surface-Enhanced Raman Spectroscopy. *Nano Lett.* **2003**, *3*, 1229–1233.
60. Brolo, A. G.; Arctander, E.; Gordon, R.; Leathem, B.; Kavanagh, K. L. Nanohole-Enhanced Raman Scattering. *Nano Lett.* **2004**, *4*, 2015–2018.
61. Robbie, K.; Friedrich, L. J.; Dew, S. K.; Smy, T.; Brett, M. J. Fabrication of Thin Films with Highly Porous Microstructures. *J. Vac. Sci. Technol. A* **1995**, *13*, 1032–1035.
62. Zhang, W.; Ganesh, N.; Block, I. D.; Cunningham, B. T. High Sensitivity Photonic Crystal Biosensor Incorporating Nanorod Structures for Enhanced Surface Area. *Sensors Actuat. B* **2007**, *131*, 279–284.
63. Homola, J. Surface Plasmon Resonance Sensors for Detection of Chemical and Biological Species. *Chem. Rev.* **2008**, *108*, 462–493.
64. Stewart, M. E.; Yao, J.; Maria, J.; Gray, S. K.; Rogers, J. A.; Nuzzo, R. G. Multispectral Thin Film Biosensing and Quantitative Imaging Using 3D Plasmonic Crystals. *Anal. Chem.* **2009**, *81*, 5980–5989.
65. Hua, F.; Gaur, A.; Sun, Y.; Word, M.; Jin, N.; Adesida, I.; Shim, M.; Shim, A.; Rogers, J. A. Processing Dependent Behavior of Soft Imprint Lithography on the 1−10-nm Scale. *IEEE Trans. Nanotechnol.* **2006**, *5*, 301–308.
66. Chang, S.-H.; Gray, S. K.; Schatz, G. C. Surface Plasmon Generation and Light Transmission by Isolated Nanoholes and Arrays of Nanoholes in Thin Metal Films. *Opt. Express* **2005**, *13*, 3150–3165.

67. Gray, S. K.; Kupta, T. Propagation of Light in Metallic Nanowire Arrays: Finite-Difference Time-Domain Studies of Silver Cylinders. *Phys. Rev. B* **2003**, *68*, 045415.
68. Maria, J.; Truong, T. T.; Yao, J.; Lee, T.-W.; Nuzzo, R. G.; Leyffer, S; Gray, S. K.; Rogers, J. A. Optimization of 3D Plasmonic Crystal Structures for Refractive Index Sensing. *J. Phys. Chem. C* **2009**, *113*, 10493–10499.
69. Shuford, K. L.; Ratner, M. A.; Gray, S. K.; Schatz, G. C. Finite-Difference Time-Domain Studies of Light Transmission through Nanohole Structures. *Appl. Phys. B: Laser Opt.* **2006**, *84*, 11–18.
70. Taflove, A.; Hagness, S. C. *Computational Electrodynamics: The Finite-Difference Time-Domain*; Artech House: Boston, MA, 2005.